INT. J. REMOTE SENSING, 1994, VOL. 15, NO. 10, 2099-2119

Indicators of land-cover change for change-vector analysis in multitemporal space at coarse spatial scales

E. F. LAMBIN* and A. H. STRAHLER

Department of Geography, Boston University, 675 Commonwealth Avenue, Boston, MA 02215, U.S.A.

(Received 20 April 1993; in final form 29 November 1993)

Abstract. Change-vector analysis in multi-temporal space is a powerful tool to analyse the nature and magnitude of land-cover change. The change vector compares the difference in the time-trajectory of a biophysical indicator for successive time periods. This change detection method is applied to three remotely-sensed indicators of land-surface conditions—vegetation index, surface temperature and spatial structure—in order to improve the capability to detect and categorize subtle forms of land-cover change. It is tested in a region of West Africa, using multi-temporal Local Area Coverage imagery obtained by the Advanced Very-High Resolution Radiometer on NOAA-9 and NOAA-11 orbiting platforms. The three indicators show a low degree of redundancy and detect different land-cover change processes, which operate at different time scales. Change vector analysis is being developed for application to the land-cover change product to be produced using NASA's Moderate-Resolution Imaging Spectroradiometer instrument, scheduled for flight in 1998 and 2000 on EOS-AM and -PM platforms.

1. Introduction

The land surface has considerable control on the planet's energy balance, biogeochemical cycles and hydrologic cycle, which in turn significantly influence the climate system. Changes in land cover are driven by five categories of causes: (1) long-term natural changes in climatic conditions, (2) geomorphological and ecological processes such as soil erosion and vegetation successions, (3) human-induced alterations of vegetation cover and landscapes, such as deforestation and land degradation, (4) interannual climatic variability, which affects primarily arid and semiarid regions, and might lead to recurrent periods of droughts accompanied by modifications in the vegetation cover, annual primary production and the hydrologic cycle and (5) hypothetically, human-induced climatic changes through an enhancement of the greenhouse effect. These fundamentally different processes also have very different effects on ecosystems and human activities, occur at different rates, and are characterized by varying degrees of reversibility. Therefore, not only is there a need for a global assessment of the changes in land-cover (IGBP 1990, Anonymous 1992), but also the exact processes of changes should be identified and categorized, to allow eventually for an ecological modelling of changes in surface conditions on a global scale. Particularly important is the discrimination between the human-induced changes and naturally-induced changes, since the first ones occur at

*Current address: Joint Research Centre, IATD/MTV TP 440, I-21020 Ispra (Varese), Italy.

0143-1161/94 $10.00

rates which are unprecedented in natural conditions and are likely to increase in importance if not controlled and/or mitigated by policy interventions. The potential of remote sensing to detect and categorize these changes at a global scale is widely recognized today (e.g. Townshend *et al.* 1991), thanks to its characteristics of scale, global coverage and temporal frequency of observation.

In this paper, we apply a change detection method described by Lambin and Strahler (1994) to different remotely-sensed indicators of land-surface conditions in order to improve the capability to detect and categorize subtle forms of land-cover changes. This method is designed for high temporal resolution data, such as those of NOAA's Advanced Very High Resolution Radiometer (AVHRR). It is developed in the context of the land-cover change product to be produced using NASA's Moderate Resolution Imaging Spectroradiometer (MODIS), an instrument planned for flight on the EOS-AM and -PM platforms in 1998, 2000, and beyond.

2. Change detection method

The land-cover change detection approach which is applied in this paper is based on a comparison of the temporal development curve, or time-trajectory, for successive years of remotely-sensed indicators derived from high temporal resolution data, such as those from AVHRR. When the time trajectory of these indicators over a particular pixel departs from that expected for that pixel, a process of land-cover change can be detected. The expected time trajectory can be derived from the past history of that pixel. In addition to allowing an unambiguous detection of abrupt changes in land-cover types, this multi-temporal approach is more sensitive to subtle changes in seasonality and ecosystem dynamics than the more classic approaches, for which only a few isolated dates from different years or seasons are compared.

The seasonal dynamic of a remotely-sensed indicator can be represented by a point in a multi-dimensional space, with the number of dimensions of this space corresponding to the number of observations n. These observations will either correspond to the maximum values of the indicator for prespecified compositing periods, or the results of a sampling through time of a continuous function that describes the shape of the time-trajectory of the indicator. The value taken by the indicator under consideration can be represented, for each pixel, by a point in the n-dimensional temporal space and is defined by a vector. The magnitude of this vector measures the accumulated value of the indicator through the year. The direction of this vector is a synthetic quantifier of the seasonal pattern of the indicator, i.e. the shape of the curve (Lambin and Strahler 1994). Every year the coordinates of the position of any pixel in the multi-dimensional temporal space can be observed. Any change in the accumulated value and/or in the seasonal dynamic of the indicator between successive years will result in a displacement of the pixel's point in the multi-dimensional space. This difference in position can be described by a change vector. The magnitude of the change vector measures the intensity of the change in land cover. It is calculated as the Euclidean distance between two points in the n-dimensional temporal space:

$$\left[\sum_{i=1}^{n}(I_1-I_2)_i^2\right]^{1/2}$$

where I_1 and I_2 are the year 1 and year 2 pixel values for the indicator I and i is the observation period during the year (e.g., for monthly composites, $n=12$). The

direction of the change vector indicates the nature of the land-cover change process. The main directions for a multi-temporal data set can be assessed using principal components analysis on the components of the change vectors (Lambin and Strahler 1994).

3. Indicators of land-cover change

3.1. *Vegetation index approach*

Lambin and Strahler (1994) tested this technique using normalized difference vegetation index data (NDVI) calculated from AVHRR data, over an area in West Africa. The NDVI is simply calculated for AVHRR data as (Band 2−Band 1)/(Band 2+Band 1). Multi-temporal NDVI data have been the main focus of most coarse-scale applications both for land-cover mapping applications (Norwine and Greegor 1983, Tucker *et al.* 1985, Thomas and Henderson-Sellers 1987, Townshend *et al.* 1987, Lloyd 1990, Loveland *et al.* 1991) and for land-cover change analysis (Malingreau *et al.* 1985, Malingreau 1986, Nelson and Holben 1986, Tucker *et al.* 1986, Hellden and Eklundh 1988, Malingreau *et al.* 1989, Hellden 1991, Tucker *et al.* 1991). Empirical studies, at a variety of spatial scales and in different ecosystems, have successfully correlated vegetation indices with variables related to (1) canopy quantities (green biomass, leaf area index, above-ground biomass, per cent canopy cover, etc.), (2) state of the vegetation (stress, vigor, chlorophyll content, etc.), (3) solar radiation interaction with plant canopies (intercepted and absorbed photosynthetically active radiation, etc.), (4) vegetation moisture (leaf water content, water satisfaction index, plant canopy water stress, etc.), (5) ecological variables (rainfall, potential and actual accumulated evapotranspiration, surface temperature) and (6) instantaneous rates associated with the activity of the vegetation (rates of photosynthesis and transpiration, minimum canopy inverse resistance to transpiration loss, net carbon dioxide exchange rate). For this last group of interpretations, time integrals of vegetation index data can provide estimates of primary production or above-ground total dry-matter accumulation. Seasonal variations of vegetation indices can be interpreted in terms of vegetation phenology (Justice *et al.* 1985) or, at a coarser spatial scale, biome seasonality and dynamics (Malingreau 1986).

While previous studies have largely emphasized the use of vegetation indices, it has been recognized that this is merely one approach to land cover/land-cover change analysis (Justice 1986). Other remotely-sensed measures, including, for example, thermal or spatial information may prove equally as important. In particular, for land-cover change detection and categorization, it can be expected that the interannual comparison of temporal development curves of a variety of independent remotely-sensed indicators will yield a greater accuracy than the analysis of a vegetation index alone. New change indicators will be helpful only if they satisfy to the following criteria. (1) Their information content should not be redundant with that of vegetation indices; rather, it should be complementary and reveal new aspects of land-cover changes. (2) They should have a clear biophysical or ecological meaning in order to facilitate the interpretation of remotely-sensed change information in terms of land-cover change processes. (3) It should be possible to derive them from remotely-sensed data at the same temporal frequency and spatial scale as the vegetation index data—ideally, from the same sensor or platform. In addition to the NDVI, two other candidate indicators will be examined in this paper: surface temperature and spatial structure.

3.2. *Land-surface temperature*

While vegetation indices are calculated from measures of reflected energy, satellite sensors can also detect the energy emitted by the surface. Several studies have shown that land-surface temperature (T_s) can be derived from AVHRR thermal channels (channels 4 and 5) using a split-window algorithm (e.g. Price 1984, Wan and Dozier 1989, Becker and Li 1990, Vidal 1991). Land-surface temperature is related, through the surface energy balance equation, to surface moisture availability and evapotranspiration, as a function of latent heat flux (e.g. Carlson *et al.* 1981, Price 1982, Seguin and Itier 1983, Taconet *et al.* 1986). A few empirical studies have demonstrated the potential of these data for land cover/land-cover change analysis. For instance, AVHRR channel 3, which is sensitive to a combination of reflected and emitted radiation, has been used to detect forest disturbances (Tucker *et al.* 1984), and to locate the boundary between shrub, tree and woodland savanna in West Africa (Malingreau *et al.* 1989) or between savanna and forest in Central Africa (Justice and Kendall, forthcoming). Land surface temperature data, derived from the thermal infrared AVHRR channels, have also been used to map the boundary between tropical rain forest and savanna vegetation (Achard and Blasco 1990). There is, however, a need for a better understanding of the biophysical factors that determine the response of vegetation in the thermal region of the spectrum at coarse spatial resolutions.

3.3. *Spatial structure of the landscape*

Patterns of surface spatial structure have a rich information content drawn from the land cover types and the processes of land-cover change. Certain categories of changes in human land use tend to fragment the landscape, such as those associated with expansion of extensive agricultural exploitation, deforestation driven by small-scale logging or farming activities, overgrazing, desertification around deep wells, growth of human settlements or urbanization. Other land-use changes increase landscape homogeneity, such as large-scale intensive cultivation or ranching. Indeed, the degree of landscape homogeneity/heterogeneity depends on the scale of analysis. The important contribution of spatial heterogeneity to ecological stability and as a controlling variable for key ecological processes is well established. Consideration of spatial patterning and the spatial dynamic of landscape have received increased attention during the past decade, as demonstrated by the development of a new field known as landscape ecology (for a review, see Turner 1989). Another reason to monitor changes in spatial structure of landscapes is that the accurate parametrization of surface processes for climate modelling requires a knowledge of the actual degree of spatial variability at the subgrid scale of some land-surface data (Henderson-Sellers and Pitman 1992).

While remote sensing studies of land cover at coarse spatial scales have largely exploited the temporal and, to a lesser extent, the spectral information, the spatial domain has often been ignored. This is understandable since global or continental AVHRR data in long time series have only been available at the Global Area Coverage (GAC) or Global Vegetation Index (GVI) resolutions, both of which suffer from artificially-introduced spatial contrast due to the spatial undersampling inherent to these data (Belward and Lambin 1990). Today however, AVHRR data are increasingly available at the full 1·1 km resolution, referred to as Local Area Average (LAC) and High Resolution Picture Transmission (HRPT) data. Even though a high sensor-induced spatial autocorrelation has been observed at this resolution (Belward

and Lambin 1990), a study based on these data has shown that different ecological zones exhibit different detectable spatial characteristics at that scale (Belward 1992). Moreover, Vogt (1992) has analysed the seasonal change in spatial structure of a West African landscape, showing that there is a marked seasonal cycle in the spatial structure of NDVI, surface temperature, and albedo, and that zones of ecological transition have an identifiable seasonal dynamic in spatial structure. Therefore, the interannual changes in the time-trajectory of an indicator of spatial structure may provide important information on land-cover change processes. This would require a good understanding of the relation between landscape structure and spatial resolution (Woodcock and Strahler 1987).

4. Data

We have tested the application of the change detection method described in Lambin and Strahler (1994) to the three remotely-sensed indicators discussed in the previous section—vegetation index, surface temperature and spatial structure—and have compared the change intensities and change categories detected by these three measures. Our test was based on AVHRR LAC data over an area in West Africa.

4.1. *Study area*

A subscene of 512 pixels by 512 pixels of LAC AVHRR data covering a region across Mali, Senegal and Guinea was selected (figure 1) (Grégoire 1990). This area includes several watersheds from the Niger, Senegal, and Gambia River systems, as well as the northern edge of the Fouta Djallon, southwest of the scene. Precipitation varies from about 1800 mm in the Fouta Djallon to 750 mm in the north of the

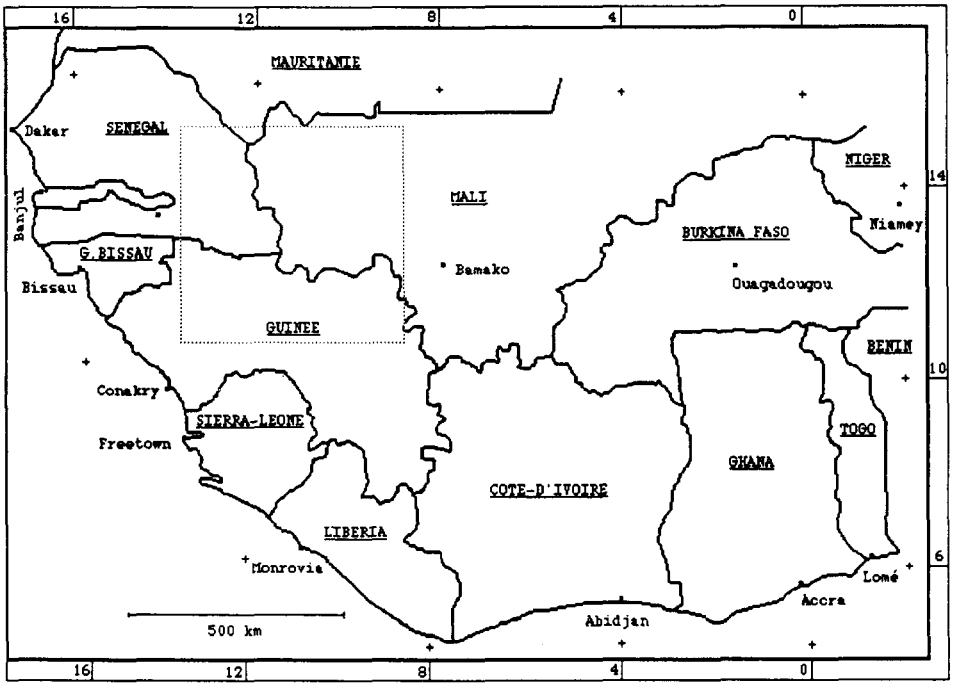

Figure 1. Location of the study area.

scene. The rainy season normally occurs from June to early October, but is shorter and starts later in the north. The area belongs to the Sudanian phytogeographic zone and, in the northern part, to the Sahelian domain. In the south, the vegetation type is open forest dominated by deciduous and semideciduous species with an herbaceous stratum, ranging to tree and shrub savannas. To the north, the herbaceous stratum dominates the landscape. The combined effect of vegetation type and climatological zoning leads to north–south variations in vegetation phenology. Vegetation senescence occurs earlier and more rapidly on the northern grass savanna than on the southern woody savanna and open forest. The patterns of vegetation growth vary similarly with vegetation types and the timing of the rains (ORSTOM 1991).

4.2. *Meteorological data*

Land-cover changes were analysed between two hydrological years (from July to June 1987/88 and 1988/89). The main interannual changes which are expected to occur in such a short interval of time are differences in the timing of vegetation activity driven by interannual variations in rainfall distribution. Monthly meteorological data for these two years were available for three different stations along the Faleme watershed, which occupies a large part of the AVHRR subscene. The rainfall and hydrological data reveal the following interannual differences (figure 2) (ORSTOM 1991):

(1) The second hydrological year (1988/89) was characterized by an earlier and more intense start of the rainy season, with a maximum in precipitation occurring in July compared to August for the first year.
(2) During the second hydrological year (1988/89), the month of October, at the end of the rainy season, was drier than the same period for the first year.

It should also be noted that a high spatial variability in rainfall distribution is typical of Sahelo-Sudanian regions (Flitcroft *et al.* 1989). The network of meteorological

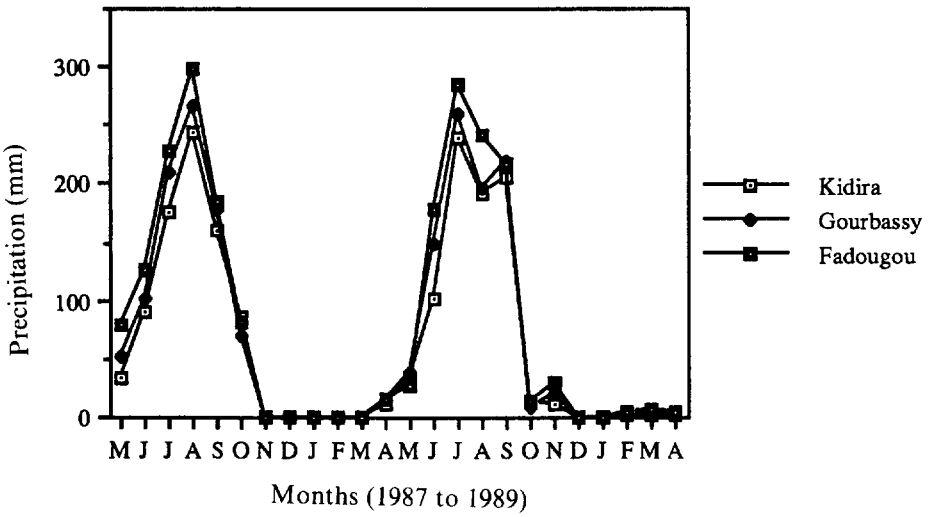

Figure 2. Monthly rainfall data at three stations in the Faleme watershed for two hydrological years.

stations is too sparse to grasp accurately the spatial variations in rainfall distribution throughout the area.

4.3. *Remotely-sensed data*

The multiyear AVHRR LAC multitemporal data used in this study were assembled and pre-processed by the Monitoring Tropical Vegetation group, at the Joint Research Center (Ispra, Italy). Data were acquired by the NOAA-9 and, after November 1988, NOAA-11 satellites. NOAA-11 has an earlier equatorial crossing time than NOAA-9. The resulting change in solar zenith angles, as well as differences in pre-launch calibration characteristics, were compensated for when calculating apparent at-satellite reflectances, by using corrections for the Sun-zenith angle, the Sun-Earth distance and the spectral response function of the sensor. For the visible and near-infrared channels, inflight calibration coefficients derived by Holben *et al.* (1990) were used. These calculations were performed using the NEWTAN software described in Vogt (1990). The calculated reflectance is a standardized value which allows a comparative analysis of values measured by different radiometers.

The data included one hundred relatively cloud- and smoke-free, near-nadir view images that were selected from the July 1987 to June 1989 period. The data were geometrically corrected to a master image using ground control points and accurately co-registered manually. Accurate registration is a key factor for successful detection of nonspurious changes in land-cover (Townshend *et al.* 1992). Three indicators were produced from the data:

(1) The normalized difference vegetation index (NDVI) was calculated from AVHRR channels 1 and 2. The atmospheric contamination and directional reflectance effects were reduced from the annual NDVI data series using the maximum-value composite technique (Holben 1986), with a one-month compositing period. This technique failed to remove all clouds, especially during the rainy season. The August composites for the two years were still largely contaminated by cloud formations and were removed from the subsequent analysis. Some other monthly composites had a few remaining clouds.

(2) The surface temperature (T_s) was derived from the brightness temperatures in AVHRR channels 4 and 5 as corrected for the gain, offset and sensor-nonlinearity of the AVHRR (Vogt 1990). The split window technique was applied using the algorithm and the coefficients described in Price (1984). This technique performs a correction for localized atmospheric variations, but does not take into account the possible effects of emissivity variations of land surfaces. The T_s data were also composited, with a one-month period, using the maximum T_s criteria. This assumes that clouds always have a lower temperature than the surface.

(3) Spatial structure was characterized by measuring the variance within an adaptive moving window applied to each NDVI monthly composite image. The size of the window was 3 pixels by 3 pixels. The moving window is adaptive, which means that the texture value for each pixel is the minimum local standard deviation value for all windows to which the pixel belongs. This technique tends to preserve edges rather than enhance them (Woodcock and Ryherd 1989). The output of this calculation is a texture image which

quantifies the local heterogeneity of the image, and represents the variability in vegetation quantities at the AVHRR LAC resolution, within a landscape unit of 3·3 km by 3·3 km. The texture image was calculated from the composited NDVI rather than from the T_s data or from original AVHRR channels, since changes in vegetation are central to most ecological processes, and are more easily interpreted than changes in T_s or in the reflectance of individual channels.

4.4. *Analytical procedures*

The change vectors between the two hydrological years were calculated for all three indicators and the images of the change vector magnitudes were compared for the three indicators. To interpret the magnitudes of the different change vectors in terms of change processes, the main directions of the change vectors in the multi-dimensional temporal space were assessed by identifying the largest interannual differences for each monthly period. In Lambin and Strahler (1994), a method, based on principal component analysis, to identify mathematically these directions is presented. In this paper, we shall restrict the discussion to the results which are directly useful to assess the relative contribution of each indicator to change detection and categorization.

5. Results

5.1. *Change-vector magnitude*

For every pixel, the temporal vectors for the two hydrological years, calculated from the monthly composites but excluding the August period, were subtracted from each other, yielding a change vector. This calculation was performed separately for the three indicators. The magnitude of the change vectors were displayed as images for the three indicators. A density slicing of these images has been produced for the NDVI (figure 3), T_s (figure 4) and spatial structure of the NDVI (figure 5), based on natural break points in their histograms. These figures provide a cartographic representation of the intensity of land-cover changes between the two years. Different intensities of change are represented on these figures:

(1) The white and yellow correspond to areas with, respectively, very large or large interannual variations. For the NDVI and T_s change images, these are related to clouds that remained after compositing. For the spatial structure and, to a lesser extent, the NDVI change images, it also corresponds to two large lakes (Manantali in the centre and Selingue in the south-east, both in Mali) which are characterized by large variations in water level between the two years.

(2) The red corresponds to areas with medium land-cover change intensities. They are restricted to some regions of the images and, on the NDVI and T_s change images, are spatially autocorrelated. Interannual variations in rainfall distribution and vegetation phenology have probably led to differences in biophysical conditions between the two years for those regions. For the spatial structure change image, these pixels with a medium change intensity have a more scattered pattern, with, however, a more frequent occurrence in the south-west part of the image.

(3) The green and blue areas correspond to, respectively, low amplitude, probably not significant, interannual changes, and the no-change category.

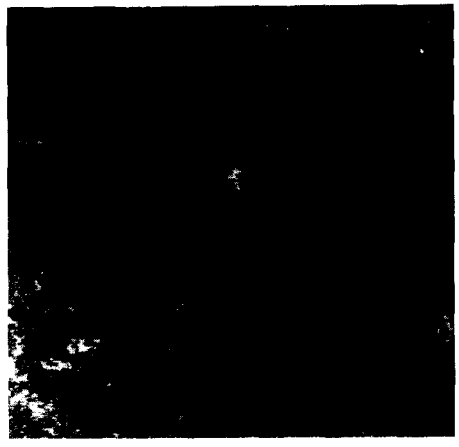

Figure 3. Density slicing of the change vector magnitude image for the NDVI. (Yellow: high change intensities; Red: medium change intensities; Green: low change intensities; Blue: no change).

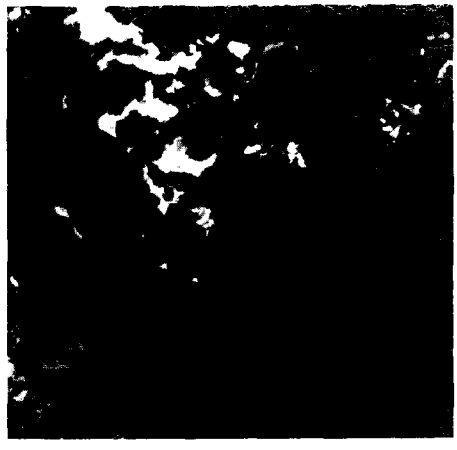

Figure 4. Density slicing of the change vector magnitude image for the Ts. (White: very high change intensities; Yellow: high change intensities; Red: medium change intensities; Green: low change intensities; Blue: no change).

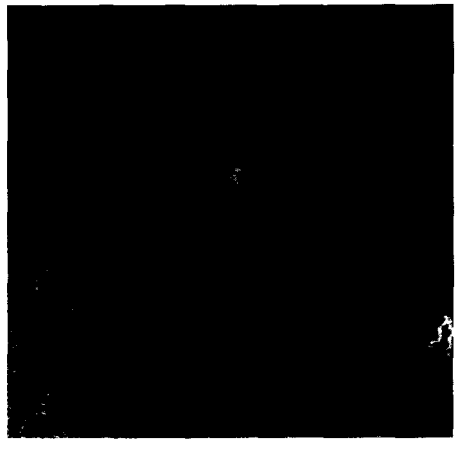

Figure 5. Density slicing of the change vector magnitude image for the spatial structure of the NDVI. (Yellow: high change intensities; Red: medium change intensities; Green: low change intensities; Blue: no change).

The fact that these four categories of change are distributed in a spatially structured and nonrandom fashion suggests that they correspond to real change processes rather than to noise or computation artifacts, which would have been spatially unstructured.

5.2. *Processes of change detected by the three indicators*

It is visually obvious that the change vector magnitude images of NDVI, T_s and spatial structure display independent types of information. This is confirmed by the values of the correlation coefficients between these three images (table 1). The NDVI and spatial structure change images are, to a certain degree, correlated ($r=0{\cdot}5$), which could be expected since the spatial structure data were derived by texturing the NDVI data. But the correlation between the change images calculated from the NDVI and T_s data, as well as between T_s and spatial structure of the NDVI data are nearly zero. This suggests that the three indicators detect different processes of change. Those will be compared next, looking at the indicators pairwise.

(a) *NDVI and T_s*

There are two main differences between the NDVI and T_s change images (figures 3 and 4). First, the NDVI and T_s best detect remaining clouds from different montly composites and located in different parts of the scene. The cloud formation in the south-west part of the image, from the October monthly composite of the first hydrological year, is clearly identified on the NDVI change image as part of the class of highest intensity changes (in yellow). On the T_s change image, it is measured as a lower intensity change. On the other hand, the larger cloud formations in the northern part of the image, from the June monthly composite of the second year, are strongly identified by T_s vectors (in white), but are not detected at all by the NDVI change vectors.

This is one illustration of the complementarity between these two biophysical indicators. In the October image the vegetation cover is at its peak greenness in the southern part of the scene. The high NDVI values contrast sharply with the very low NDVI over clouds (figure 6), leading to a good detection of these clouds as an interannual change (figure 3). The T_s over vegetation is minimum at that period, due to the high rate of evapotranspiration of vegetation which increases the latent heat flux and leads to a cooling of the surface. Therefore, on the T_s image, the cold cloud formations do not contrast as well as on the NDVI image with the background vegetation and is only detected as a lower intensity change (figure 4).

Table 1. Correlation coefficients between the three change vector magnitude images.

	Correlation coefficient	
	Between variables[a]	Between change vectors
NDVI – T_s	−0·55	0·04
NDVI—Spatial Structure of the NDVI	0·27	0·53
T_s—Spatial Structure of the NDVI	−0·31	−0·02

[a] Average correlation coefficient for all monthly composites (excluding August) for one year.

Figure 6. NDVI monthly composite for October, first year.

In the June image, the opposite situation occurs. The NDVI is at its minimum in the northern part of the image, since the June monthly image of the second year is mostly composed of values selected from an image recorded on 2 June, as the other images from that month were severely contaminated by clouds. In early June, rains are just starting in the northern part of the image, with not much vegetation activity yet. Therefore, the low NDVI over clouds is not separable from the low NDVI of the background. At the opposite, in June, T_s is close to its maximum for this northern area, leading to a saturation of the sensor's signal (at 320 K, or 47°C). These high land surface temperatures contrast very sharply with the low temperatures of clouds (figure 7). As a consequence, those clouds are very well detected by the T_s as interannual changes but are not detected at all by the NDVI.

Secondly, when comparing the NDVI and T_s change images, there are clear differences in the location and spatial pattern of the category of medium change intensities displayed in red. The nature of these differences may be assessed by looking at the monthly difference images that account for the change vectors magnitudes. For example, medium intensity changes are measured by the T_s change vector in the south-east part of the scene (figure 4), but are not detected by the NDVI change vector (figure 3). On the T_s change image, they appear as very large, homogeneous red patches. By analyzing the monthly difference images, these

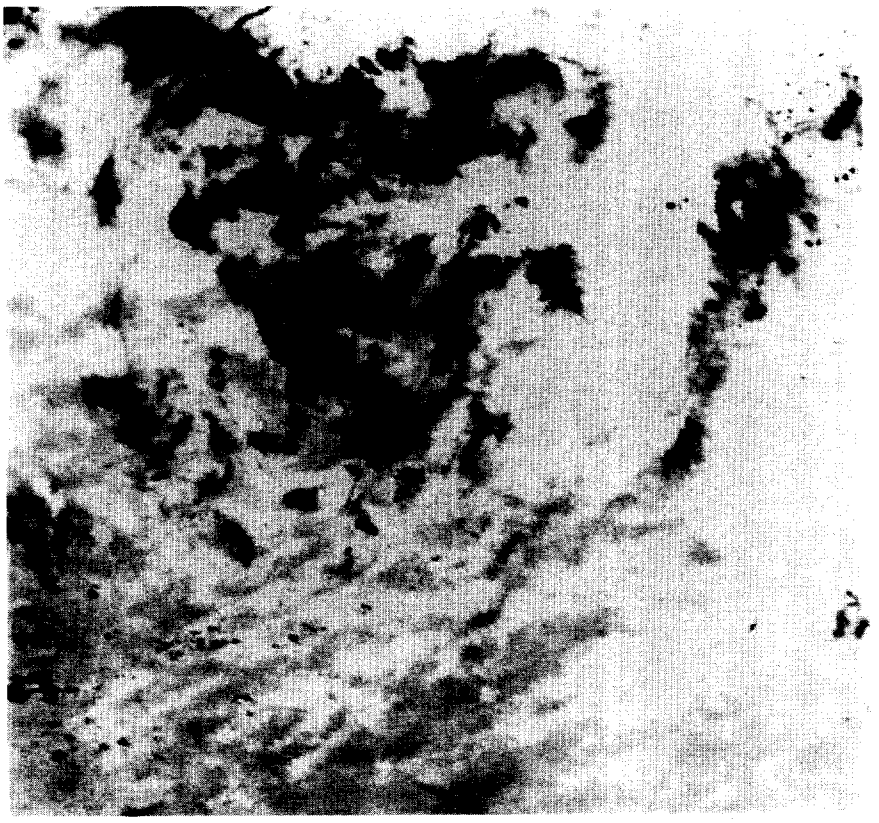

Figure 7. Ts monthly composite for June, second year.

patches are identified as corresponding to areas which have a much cooler temperature on the June monthly composite image of the first year (figure 8), compared to the second year (figure 7). Since this period corresponds to the beginning of the rainy season in the southern part of the scene, the cold surface temperatures were likely caused by high rainfall during that month, which led to an evaporative cooling of the surface. The NDVI monthly composite for the same period and the same year does not show a consistently higher NDVI for this area. This is in agreement with previous studies which have reported a marked time lag between rainfall and NDVI of some weeks, particularly at the beginning of the growing season (Malo and Nicholson 1990, Justice *et al.* 1991). This explains why these cooler regions are not detected as change by the NDVI indicator. The NDVI probably detects interannual differences in the next monthly period (July) as a result of differential vegetation growth induced by the increased water availability. This could not be verified since our data set ends in June and, therefore, we have no data for July 1989.

In general, the T_s indicator detects more ecological change in the northern part of the scene, where the vegetation cover is low, than the NDVI does. This might be explained by the fact that in the Sahelian region, the ecological dynamic is primarily driven by rainfall at the beginning of the growing season, since soil moisture

Figure 8. Ts monthly composite for June, first year.

availability is the main factor limiting vegetation growth. In the Sudanian zone though, in the southern part of the scene, the vegetation cover is denser and rainfall is less a limiting factor, even though rainfall distribution still plays an important role in the ecosystem dynamic. As a result, most of the ecological dynamic is related to vegetation phenology throughout the growing season, which is better indicated by the NDVI.

(b) *NDVI and spatial structure of the NDVI*

As stated before, the NDVI and spatial structure change images are correlated to a certain degree. They both show the largest amplitude of change in the southwest part of the scene (figures 3 and 5). However, the low intensity changes indicated by the NDVI change vectors in the centre and northern parts of the image (in green) are not as well detected by the spatial structure indicator. An analysis of the change vector components reveals that most of the interannual changes in spatial structure can be accounted for by changes in the periods of vegetation senescence and vegetation growth in the southern part of the scene, where the vegetation type is open forest and tree savanna. At the spatial resolution of AVHRR LAC data, the local variance measures change in spatial structure at the scale of the landscape. Changes in fractional vegetation cover related to the different phenological stages of the vegetation cover are indeed not detected at such a coarse spatial resolution.

To help understand the relationship between interannual variations in spatial structure and in NDVI, we have analysed the seasonal dynamic of the mean local variance, for the two years, for two 40 pixel by 40 pixel areas (figures 9 (*a*) and (*b*)), knowing that the time trajectories of NDVI follows closely vegetation's phenological cycle. The first area, from the southern part of the scene, belongs to a Sudanian landscape dominated by tree savanna. The second area, from the northern part of the scene, belongs to a Sahelian landscape, dominated by a herbaceous cover. The following observations can be made when comparing these two graphs:

(1) Most of the year, the local variance is lower for the Sahelian subimage than for the Sudanian sub-image.

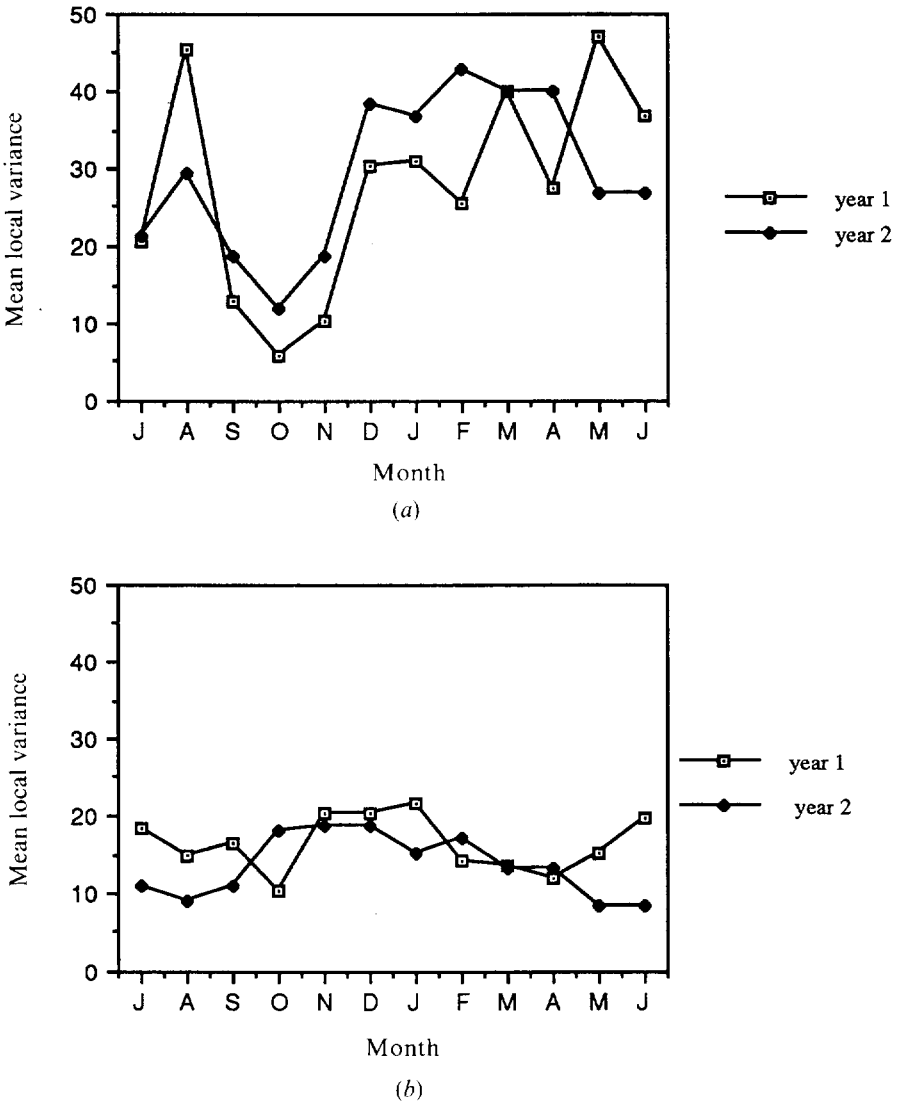

Figure 9. (*a*) Seasonal dynamic of spatial structure of the NDVI of a Sudanian landscape (South); (*b*) Seasonal dynamic of spatial structure of the NDVI of a Sahelian landscape (North).

(2) There are few seasonal variations in local variance for the subimage corresponding to the Sahelian landscape. A slight increase in spatial heterogeneity can be observed during the dry season for both years.
(3) For the Sudanian landscape, the spatial structure of the NDVI, at the AVHRR LAC spatial resolution, displays a marked seasonality, with a minimum spatial heterogeneity during the period of highest vegetation development (September to November in that region).
(4) For the Sahelian subimage, the maximum interannual difference in mean local variance is observed for the period of vegetation growth (June to August in the north). For the Sudanian subimage, interannual differences are larger and observed throughout the year, but with maxima in the periods of vegetation growth also (May to August in the south) and vegetation senescence (December to February). These are the same periods for which the larger interannual differences were detected by the NDVI (Lambin and Strahler 1994).

Thus, it appears that, for tree savanna landscapes, spatial structure varies with the phenological state of vegetation, and therefore with the seasonality of the NDVI. In contrast, in the Sahelian north, where the herbaceous stratum dominates the landscape, the state of the vegetation has less influence on the spatial structure of the landscape. This difference can be explained by the fact that in the Sudanian landscape there are more topographic effects than in the north, the human occupation of the land is more intensive and diversified, and the landscape is intrinsically more fragmented due to the presence of valley bottoms, fields, lateritic duricrusts and open forests. This heterogeneity is masked when the vegetation is fully developed throughout the landscape, but becomes apparent during the dry season and at the periods of vegetation transition, when each vegetation type is at a different stage of development or when the agricultural fields have been harvested while the natural vegetation is still green.

Therefore, the spatial structure indicator is better at detecting interannual changes in the seasonal ecosystem dynamic for spatially heterogeneous landscapes. This explains why the spatial structure of the NDVI change vector detects about the same changes as those detected by the NDVI change vectors in the southern part of the scene, but does not detect as many changes as the NDVI does in the northern part of the scene.

However, the real usefulness of a spatial indicator of changes probably does not lie in the identificaton of seasonal changes—a task that is better performed with the NDVI—but in the detection of longer term, possibly anthropogenic processes of change, which are likely to affect more drastically the landscape's spatial structure. This should be tested on longer-term time series on landscapes subject to significant transformation of vegetation cover. To summarize, NDVI and the spatial structure of the NDVI are slightly redundant as indicators of land-cover change, but this study is unable to reveal the full potential of the spatial structure indicator, which is to detect more fundamental changes in landscape ecology, such as those brought by human transformation of the land cover.

(c) *T_s and spatial structure of the NDVI*

Our analysis reveals that there is no correlation between the interannual changes in time-trajectory of T_s and the interannual changes in time-trajectory of the spatial structure of the NDVI (table 1). This means that these two indicators detect

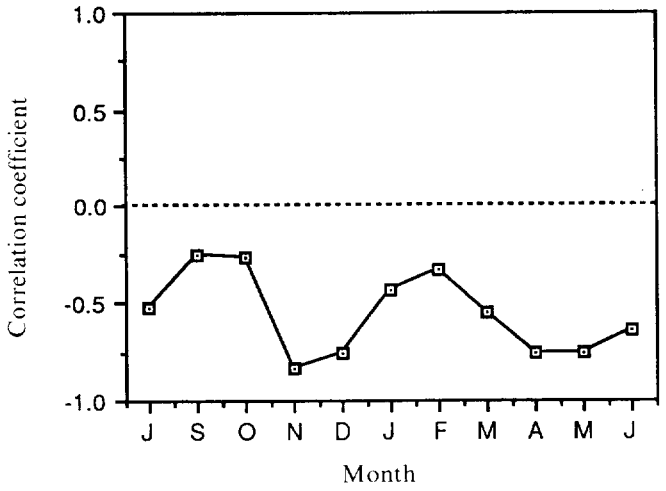

Figure 10. Correlation between monthly composited NDVI and Ts images (first year, excluding August).

independent processes of change, at the scale at which the spatial structure of the surface is represented on AVHRR LAC data.

6. Discussion

(1) The change vector analysis applied to NDVI, T_s and spatial structure of the NDVI data seem to be effective in detecting interannual land-cover changes over a West African study area. A better knowledge of actual ground conditions would be required to validate further our results. In any case, the three remotely-sensed indicators used show a low degree of redundancy and are independent.

(2) There is also a strong complementarity between the NDVI and T_s data for the task of separating cloud formations from the surface background. In the ecosystem conditions of our study area, NDVI data are better at detecting clouds when the vegetation is at its maximum activity. T_s is more effective when there is no or little vegetation activity and the surface is warm. However, overall, the T_s data are a better discriminator of clouds than the NDVI data since, in the two situations, clouds were detected, which was not the case with the NDVI data. Therefore, these empirical results suggest that it would be advantageous to apply the maximum value compositing technique on the T_s rather than on the NDVI data, and to derive the NDVI composited images by retaining, for each pixel, the dates selected by the T_s compositing. This preliminary conclusion should, however, be supported by further analyses, taking into account atmospheric versus surface temperatures in different conditions, directional reflectance effects and viewing angles.

(3) Recent studies have shown that there is a strong negative relationship between NDVI and T_s data (e.g. Goward *et al.* 1985, Nemani and Running 1989, Goward and Hope 1990, Carlson *et al.* 1990, Smith and Choudhury 1991). As shown on figure 10, a negative correlation is also found for this

dataset, in most of the monthly composite images. However, as stated in a previous section, there is no correlation between the change vector magnitude images calculated from NDVI and T_s data (table 1). Neither is there a strong correlation between the NDVI and T_s monthly difference images (figure 11), with the exception of the May and June months, which correspond to the start of the rainy season in the southern part of the scene. We can therefore conclude that, even though there is a negative correlation between spatial variations in NDVI and T_s, interannual changes in these two variables are not correlated. This suggests that, in the specific ecological context of our study area, the changes in NDVI and T_s are driven by different ecological processes. Variations in NDVI are largely driven by changes in rates of vegetation activity, a seasonal and progressive process with a high degree of temporal autocorrelation. No abrupt changes in the seasonal development of vegetation are expected, unless exogeneous events such as drought, fire or anthropogenic clearing occur. In contrast, variations in T_s in semiarid or dry subhumid ecosystems, where the fractional vegetation cover is low, are mainly driven by rainfall events, leading to short-term, erratic variations in soil moisture and evaporative cooling. The time scale of variation of these two variables is therefore different, which explains the lack of correlation betwee their patterns of interannual changes.

(4) Among the three indicators which have been analysed in this study, spatial structure will probably best reveal longer-term and longer-lasting changes in landscape ecology, such as those related to the permanent clearing of natural vegetation by human activity. Our results clearly demonstrate that the spatial structure calculated from remotely-sensed data is not a static measure. Like the NDVI or T_s, it displays significant seasonal variation. Therefore, to detect processes of change that alter the landscape ecology, it is essential to compare the time-trajectory of spatial structure between different years rather than spatial structure data derived from single dates. This is even more

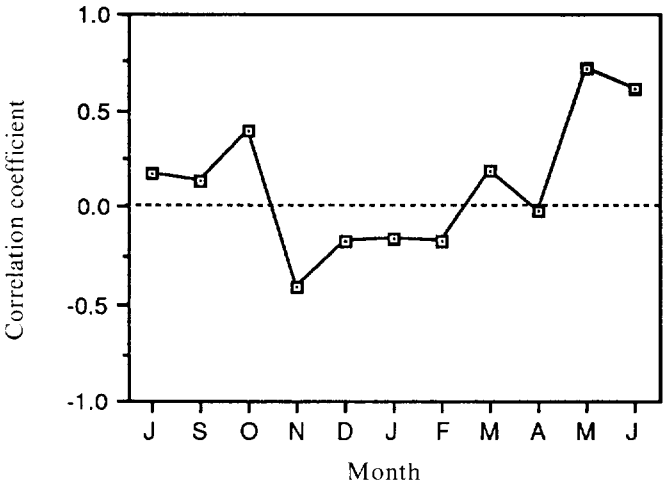

Figure 11. Correlation between NDVI and T_s monthly difference images (excluding August).

important for spatially heterogeneous landscapes. Further tests should be conducted on this indicator.

(5) Different techniques can be used to integrate the changes detected by several indicators. The most appropriate technique of integration depends primarily on the goal of the study: unsupervised clustering to synthesize the independently-derived land-cover change information, colour compositing to display it in an analytic form, or separate analysis of the three change images to sort out different processes of change. These are subjects of current research.

7. Conclusion

The potential of vegetation indices, land surface temperatue, and spatial structure to detect and categorize land-cover change has been analysed and compared. The three indicators detect different land-cover change processes, which operate at fundamentally different time scales. The time scale of variability of the processes detected by the T_s is short. Its analysis is limited by the compositing period. It responds to short-term variations in energy balance, related to rainfall events and changes in soil moisture. The NDVI detects interannual variations in processes occurring at the scale of the season, such as vegetation growth and senescence, though it can also detect abrupt changes in vegetation activity. Spatial structure is more likely to detect long term processes related to structural changes in landscape ecology. We therefore recommend that, whenever possible, the three indicators should be combined for an accurate detection and categorization of changes in land cover. Their combination should also improve the detection of changes due to residual atmospheric cloud contamination. This 'multi-information' approach is particularly easy to implement when, as it is the case with AVHRR, these different indicators can be derived from the same sensor, i.e. at the same scale, temporal frequency and viewing angle.

The analysis we present here is being developed in the context of the land-cover change product to be provided by NASA's Earth Observing System using the Moderate Resolution Imaging Spectroradiometer (MODIS) (Salomonson *et al.* 1989). This instrument is similar to the AVHRR sensor in that it will provide frequent temporal coverage of the earth, acquiring images on a two-day repeat. It will acquire data in 36 spectral bands at spectral resolutions ranging from 250 m to 1 km. MODIS is now scheduled for flight on both EOS-AM and -PM platforms, due for launch in 1998 and 2000, respectively.

Acknowledgments

We warmly thank Jean-Paul Malingreau and Jean-Marie Grégoire (Joint Research Center, Ispra, Italy) for providing us with the AVHRR data set they assembled in the framework of the activities of the Monitoring Tropical Vegetation Group. We also thank Joe Lenart for his help in processing the data. This work was partially supported by NASA under contract NAS5-31369 (Earth Observing System).

References

ACHARD, F., and BLASCO, F., 1990, Analysis of vegetation seasonal evolution and mapping of forest cover in West Africa with the use of NOAA AVHRR HRPT data. *Photogrammetric Engineering and Remote Sensing*, **56**, 1359–1365.

ANONYMOUS (1992), Land Use and Land Cover Change. *AMBIO*, **21,** 122.

BECKER, F., and LI, Z.-L., 1990, Towards a local split window over land surfaces. *International Journal of Remote Sensing*, **11,** 369–393.

BELWARD, A. S., and LAMBIN, E. F., 1990, Limitations to the identification of spatial structures from AVHRR data. *International Journal of Remote Sensing*, **11,** 921–927.

BELWARD, A. S., 1992, Spatial attributes of AVHRR imagery for environmental monitoring. *International Journal of Remote Sensing*, **13,** 193–208.

CARLSON, T. N., DODD, J. K., BENJAMIN, S. G., and COOPER, J. N., 1981, Remote estimation of surface energy balance, moisture availability and thermal inertia. *Journal of Applied Meteorology*, **20,** 67–87.

CARLSON, T. N., PERRY, E. M., SCHMUGGE, T. J., 1990, Remote estimation of soil moisture availability and fractional vegetation cover over patchy vegetation. *Agricultural and Forest Meteorology*, **52,** 44–60.

FLITCROFT, I. D., MILFORD, J. R., and DUGDALE, G., 1989, Relating point to area average rainfall in semiarid West Africa and the implications for rainfall estimates derived from satellite data. *Journal of Applied Meteorology*, **28,** 252–266.

GOWARD, S. N., CRUICKSHANKS, G. D., and HOPE, A. S., 1985, Observed relation between thermal emission and reflected spectral radiance of a complex vegetated landscape. *Remote Sensing of Environment*, **18,** 137–146.

GOWARD, S. N., and HOPE, A. S., 1990, Evapotranspiration from combined reflected solar and emitted terrestrial radiation: Preliminary FIFE results from AVHRR data. *Advances in Space Research*, **9,** 239–249.

GRÉGOIRE, J. M., 1990, Effects of the dry season on the vegetation canopy of some river basins of West Africa as deduced from NOAA-AVHRR data. *Hydrological Sciences Journal*, **35,** 323–337.

HELLDEN, U., and EKLUNDH, L., 1988, National Drought Impact Monitoring. A NOAA NDVI and precipitation data study of Ethiopia. *Lund Studies in Geography*, Ser. C., No. 15, Lund University Press, Sweden, 55p.

HELLDEN, U., 1991, Desertification—Time for an Assessment? *AMBIO*, **20,** 372–383.

HENDERSON-SELLERS, A., and PITMAN, A. J., 1992, Land-Surface Schemes for Future Climate Models: Specification, Aggregation, and Heterogeneity. *Journal of Geophysical Research*, **97D,** 2687–2696.

HOLBEN, B. N., 1986, Characteristics of maximum-value composite images from temporal AVHRR data. *International Journal of Remote Sensing*, **7,** 1417–1434.

HOLBEN, B. N., KAUFMAN, Y. J., and FRASER, R. S., 1990, NOAA-11 AVHRR visible and near-IR inflight calibration. *International Journal of Remote Sensing*, **11,** 1511–1519.

IGBP (International Geosphere Biosphere Programme), 1990, *The International Geosphere Biosphere Programme: A Study of Global Change*. The Initial Core Projects Report No. 12, International Council of Scientific Unions, Stockholm, Sweden.

JUSTICE, C. O., TOWNSHEND, J. R., HOLBEN, B. N., and TUCKER, C. J., 1985, Analysis of the phenology of global vegetation using meteorological satellite data. *International Journal of Remote Sensing*, **6,** 1271–1318.

JUSTICE, C. O., 1986, Monitoring the grasslands of semi-arid Africa using NOAA AVHRR data, Editorial. *International Journal of Remote Sensing*, **7,** 1385–1390.

JUSTICE, C. O., DUGDALE, G., TOWNSHEND, J. R., NARRACOTT, A. S., and KUMAR, M., 1991, Synergism between NOAA-AVHRR and Meteosat data for studying vegetation development in semi-arid West Africa. *International Journal of Remote Sensing*, **12,** 1349–1368.

JUSTICE, C. O., and KENDALL, J. D., forthcoming, Assessment of the forests of Central Africa using coarse resolution satellite data.

LAMBIN, E. F., and STRAHLER, A. H., 1994, Change-vector analysis in multitemporal space: a tool to detect and categorize land-cover change processes using high temporal-resolution satellite data. *Remote Sensing of Environment*, in press.

LLOYD, D., 1990, A phenological classification of terrestrial vegetation cover using shortwave vegetation index imagery. *International Journal of Remote Sensing*, **11,** 2269–2279.

LOVELAND, T. R., MERCHANT, J. W., OHLEN, D. O., and BROWN, J., 1991, Development of a land-cover database for the conterminous U.S., *Photogrammetric Engineering and Remote Sensing*, **57,** 1453–1463.

MALINGREAU, J. P., STEPHENS, G., FELLOWS, L., 1985, Remote Sensing of Forest Fires: Kalimantan and North Borneo in 1982–83. *AMBIO*, **14,** 314–321.

MALINGREAU, J. P., 1986, Global vegetation dynamics: satellite observations over Asia. *International Journal of Remote Sensing*, **7,** 1121–1146.

MALINGREAU, J. P., 1989, The vegetation index and the study of vegetation dynamics. In *Applications of remote sensing to agrometeorology*, edited by F. Toselli (Commission of European Community & European Space Agency, Brussels), pp. 285–303.

MALINGREAU, J. P., TUCKER, C. J., and LAPORTE, N., 1989, AVHRR for monitoring global tropical deforestation. *International Journal of Remote Sensing*, **10,** 855–867.

MALO, A. D., and NICHOLSON, S. E., 1990, A study of rainfall and vegetation dynamics in the African Sahel using normalized difference vegetation index. *Journal of Arid Environments*, **19,** 1–24.

NELSON, R., and HOLBEN, B., 1986, Identifying deforestation in Brazil using multiresolution satellite data. *International Journal of Remote Sensing*, **7,** 429–448.

NEMANI, R. R., and RUNNING, S. W., 1989, Estimation of regional resistance to evapotranspiration from NDVI and Thermal-IR AVHRR data. *Journal of Applied Meteorology*, **28,** 276–284.

NORWINE, J., and GREEGOR, D. H., 1983, Vegetation classification based on Advanced Very High Resolution Radiometer (AVHRR) satellite imagery. *Remote Sensing of Environment*, **13,** 67–87.

ORSTOM (Institut Francais de Recherche Scientifique pour le Développement en Coopération), 1991, *Conséquences hydrologiques des changements d'états de surface survenant sur les basins des grands fleuves d'Afrique de l'Ouest*. Rapport final des phases I et II, Contrat no. 3840-89-11 ED ISP F avec le Centre Commun de Recherche d'Ispra-IATD, Montpellier, France.

PRICE, J. C., 1982, On the use of satellite data to infer surface fluxes at meteorological scales. *Journal of Applied Meteorology*, **21,** 1111–1122.

PRICE, J. C., 1984, Land surface temperature measurements from the split-window channels of the NOAA 7 Advanced Very High Resolution Radiometer. *Journal of Geophysical Research*, **89 D,** 7231–7237.

SALMONSON, V. V., BARNES, W. L., MAYMON, P. W., MONTGOMERY, H. E., and OSTROW, H., 1989, MODIS: Advanced facility instrument for studies of the Earth as a system. *I.E.E.E. Transactions on Geoscience and Remote Sensing*, **27,** 145–153.

SEGUIN, B., and ITIER, B., 1983, Using midday surface temperature to estimate daily evaporation from satellite thermal IR data. *International Journal of Remote Sensing*, **4,** 371–383.

SMITH, R. C. G., and CHOUDHURY, B. J., 1990, On the correlation of indices of vegetation and surface temperature over south-eastern Australia. *International Journal of Remote Sensing*, **11,** 2113–2120.

TACONET, O., CARLSON, T. N., BERVARD, R., and VIDAL-MADJAR, D., 1986, Evaluation of a surface/vegetation parametrization using satellite measurements of surface temperature. *Journal of Climate and Applied Meteorology*, **25,** 1752–1767.

THOMAS, G., and HENDERSON-SELLERS, A., 1987, Evaluation of satellite derived land-cover characteristics for global climate modelling. *Climate Change*, **11,** 313–348.

TOWNSHEND, J. R., JUSTICE, C. O., and KALB, V., 1987, Characterization and classification of South American land cover types using satellite data. *International Journal of Remote Sensing*, **8,** 1189–1207.

TOWNSHEND, J. R. G., JUSTICE, C., LI, W., GURNEY, C., and MCMANUS, J., 1991, Global Land-Cover classification by remote sensing: present capabilities and future possibilities. *Remote Sensing of Environment*, **35,** 243–255.

TOWNSHEND, J. R. G., JUSTICE, C. O., GURNEY, C., and MCMANUS, J., 1992, The impact of misregistration on the detection of changes in land-cover. *I.E.E.E. Transactions on Geosciences and Remote Sensing*, **30(5),** 1054–1060.

TUCKER, C. J., HOLBEN, B. N., and GOFF, T. E., 1984, Intensive Forest Clearing in Rondonia, Brazil, as Detected by Satellite Remote Sensing. *Remote Sensing of Environment*, **15,** 255–261.

TUCKER, C. J., TOWNSHEND, J. R., and GOFF, T. E., 1985, African land-cover classification using satellite data. *Science*, **224,** 369–375.

TUCKER, C. J., JUSTICE, C. O., and PRINCE, S. D., 1986, Monitoring the grasslands of the Sahel 1984–1985. *International Journal of Remote Sensing*, **7,** 1571–1581.

TUCKER, C. J., DREGNE, H. E., and NEWCOMB, W. W., 1991, Expansion and Contraction of the Sahara Desert from 1980 to 1990. *Science*, **253,** 299–301.

TURNER, M. G., 1989, Landscape ecology: The effect of pattern on process. *Annual Review in Ecology and Systematics*, **20,** 171–197.

VIDAL, A., 1991, Atmospheric and emissivity correction of land surface temperature measured from satellite using ground measurements or satellite data. *International Journal of Remote Sensing*, **12,** 2449–2460.

VOGT, J., 1990, *Calculation of t-o-a albedo, NDVI, surface temperature, and precipitable water content of the atmosphere from NOAA AVHRR data*. Technical Note 1.90.72, Commission of the European Communities, Joint Research Centre, Ispra, Italy, 29p.

VOGT, J., 1992, Characterizing the spatio-temporal variability of surface parameters from NOAA-AVHRR data. Report EUR 14637 EN, Agriculture Series, Joint Research Centre, Institute for Remote Sensing Applications, 266p.

WAN, Z., and DOZIER, J., 1989, Land-surface temperature measurement from space: physical principles and inverse modelling. *I.E.E.E. Transactions on Geosciences and Remote Sensing*, **GE-27,** 268–277.

WOODCOCK, C. E., and STRAHLER, A. H., 1987, The factor of scale in remote sensing. *Remote Sensing of Environment*, **21,** 311–325.

WOODCOCK, C. E., and RYHERD, S. L., 1989, Generation of texture images using adaptive windows. *Technical Papers, 55th Annual Meeting ASPRS, Vol. 2, at Baltimore, Maryland, on 2–7 April 1989* (Bethesda, Maryland: ASPRS), pp. 11–22.